Faculty of Science and Engineering

School of Geography, Earth and Environmental Sciences

2019-10-31

# The interplay between regeneration and scavenging fluxes drives ocean iron cycling

# Tagliabue, A

http://hdl.handle.net/10026.1/15111

10.1038/s41467-019-12775-5
Nature Communications
Springer Science and Business Media LLC

All content in PEARL is protected by copyright law. Author manuscripts are made available in accordance with publisher policies. Please cite only the published version using the details provided on the item record or document. In the absence of an open licence (e.g. Creative Commons), permissions for further reuse of content should be sought from the publisher or author.

# The interplay between regeneration and scavenging fluxes drives ocean iron cycling

- Alessandro Tagliabue<sup>1\*</sup>, Andrew R. Bowie<sup>2</sup>, Timothy DeVries<sup>3</sup>, Michael J. Ellwood<sup>4</sup>, William M. Landing<sup>5</sup>, Angela Milne<sup>5,6</sup>, Daniel C. Ohnemus<sup>7</sup>, Benjamin S. Twining<sup>8</sup> and Philip W. Boyd<sup>2</sup>
- School of Environmental Sciences, University of Liverpool, Liverpool, United Kingdom
   Institute for Marine and Antarctic Studies and Antarctic Climate and Ecosystems CRC.
- 9 University of Tasmania, Australia
  - 3. University of California Santa Barbara, Santa Barbara, USA
- 4. Research School of Earth Sciences, Australian National University, Canberra, Australia
- 12 5. Florida State University, Tallahassee, Florida, USA.
- 13 6. Plymouth University, Plymouth, United Kingdom
  - 7. Skidaway Institute of Oceanography, Georgia, USA
  - 8. Bigelow Laboratory for Ocean Science, Maine, USA
  - \*corresponding author: a.tagliabue@liverpool.ac.uk

### **Abstract:**

Despite recent advances in observational data coverage, quantitative constraints on how different physical and biogeochemical processes shape dissolved iron distributions remain elusive, lowering confidence of future projections in iron-limited regions. Here we show that dissolved iron is cycled rapidly in Pacific mode and intermediate water and accumulates at a rate controlled by the strongly opposing fluxes of regeneration and scavenging. Combining new datasets within a watermass framework shows that the multidecadal iron accumulation is much lower than expected from a meta-analysis of iron regeneration fluxes. This mismatch can only be reconciled by invoking significant rates of iron removal operating on multidecadal timescales, which imply generation of authigenic iron pools. Consequently, the rapid internal cycling of iron, rather than its physical transport, is the main control on observed iron stocks within intermediate waters globally and upper ocean iron limitation will be strongly sensitive to subtle changes to the internal cycling balance.

# <u>Introduction</u>

Upper ocean primary production is limited by the availability of iron (Fe) over much of the ocean<sup>1</sup>. Even where nitrogen (N) and phosphorus (P) are the main limiting factors, Fe continues to play a key role by driving rates of N fixation<sup>2</sup> and acquisition of dissolved organic P<sup>3</sup>. Fe limitation ultimately arises due to a deficiency in the supply of Fe, relative to N and P<sup>4</sup>. Away from regions of dust deposition, the dominant component of Fe delivery, relative to N or P, is its relative concentration in thermocline waters<sup>5</sup>. This is particularly apparent across the south Pacific Ocean, where transport by sub-Antarctic mode water (SAMW) and Antarctic Intermediate water (AAIW) plays a key role in setting thermocline nutrient levels<sup>6</sup>. Accordingly, any fluctuations in the relative balance between Fe and major nutrients N and P in mode and intermediate waters in response to changes in climate will influence upper ocean Fe limitation and consequently modify global carbon and nitrogen cycles.

At present, there is low confidence in model projections of how modulations to climate will affect Fe supply to the upper ocean, as models generally show poor skill and substantial

disagreement in their representation of the present-day ocean iron cycle. This lack of fundamental understanding of iron biogeochemistry is well illustrated by the order of magnitude inter-model variability in the residence time of iron in global models, despite aiming to reproduce the same ocean distributions and patterns from state of the art datasets<sup>7</sup>. Thus, despite a relatively long legacy of modelling the ocean iron cycle<sup>8,9</sup>, significant uncertainties in the magnitude of the major processes remain<sup>1,10</sup>. This means that while shifts in Fe inventories may indeed drive end-of-century trends in simulated productivity across much of the global ocean<sup>11-15</sup>, confidence in model projections is diminished by the lack of mechanistic constraints on their behaviour.

The ocean iron cycle is affected by an array of processes that interact together to set the dissolved iron concentrations in different parts of the ocean<sup>16</sup>. In the past decade, continental margins and hydrothermal vents have been acknowledged to augment dust deposition as important external iron sources 17,18. Perhaps most striking has been the recognition that the internal cycling of iron is typified by a range of biotic and abiotic transformations linked to Fe uptake, recycling, regeneration, scavenging and colloidal dynamics 10,19. These processes act to shuttle dissolved iron between soluble and colloidal phases<sup>20-22</sup> and drive transitions of particulate iron between biogenic, lithogenic and authigenic (i.e., the residual particulate Fe not accounted for by lithogenic and algal biogenic pools) components 23,24. Despite these new insights, the relative magnitude of regeneration and scavenging, and crucially, the realised rate of net regeneration, is unknown at the spatial and temporal scales of mode and intermediate water transport. In part due to these missing constraints, global ocean models used to assess the response of ocean ecology, biogeochemistry and the carbon cycle to environmental change are free to tune their internal iron cycle with residence times that vary from a few tens to a few hundreds of years'.

 Newly expanded datasets of dissolved Fe (DFe) distributions from international ocean survey efforts within the GEOTRACES programme<sup>25,26</sup> should facilitate model improvement, but only if quantitative insights into the governing processes can be determined. A particular challenge is to disentangle the balance between biogeochemical and physical processes in setting nutrient levels in the oceans' interior. For example, total phosphate (PO<sub>4</sub>) at depth is made of up of two components: one associated with physical transport to depth (preformed PO<sub>4</sub>) and the other from the regeneration of P from organic matter degradation (regenerated PO<sub>4</sub>) which is quantified using apparent oxygen utilisation (AOU)<sup>27,28</sup>. A similar framework can be outlined for Fe, but Fe may be decoupled from P as it is affected by additional processes, such as extra Fe inputs onto intermediate water surfaces, unique regeneration of Fe, or Fe removal by scavenging<sup>1,10,29</sup>. While scavenging of Fe will add complexity to the two component model used for P, its magnitude remains an unknown quantity. This lack of understanding is encapsulated by our evolving view of the ocean iron residence time<sup>7,30,31</sup>.

Here we use observations to quantify the modification of DFe, benchmarked to PO<sub>4</sub>, within the mode and intermediate waters of the south Pacific Ocean, using AOU to derive the role played by physics, regeneration and scavenging for the first time. We focus on mode and intermediate waters as they support the majority of global productivity through nutrient supply to surface waters<sup>6</sup>. This approach illuminates a highly dynamic interior ocean Fe cycle is, within which the commonly measured DFe pool is only a small residual component. Consequently, additional measurements of the ocean iron cycle pools beyond DFe and in particular fluxes are necessary to better constrain internal cycling and reduce uncertainty in global climate model projections.

# **Results**

#### Tracking South Pacific iron and phosphate accumulation

Pacific Ocean SAMW and AAIW form in the southeast Pacific Ocean<sup>32,33</sup> and their equatorward transport is well sampled by the southern part of the CLIVAR P16 cruise track along 150W (Figure 1, Supplementary Figure 1). We targeted the region 46-10S of the transect within a potential density window of 26.8-27.2 that broadly encompasses both SAMW and AAIW (hereafter defined as intermediate water)<sup>32,34</sup>. In this density window, salinity was relatively well conserved at 34.3-34.5 (indicating negligible mixing from multiple end-members), and enough parallel observations of DFe, PO<sub>4</sub> and oxygen needed for our analysis were available (n=89). As intermediate water moves equatorward its core depth varies between 200m to 800m and AOU increases from 20 to 160 mmol m<sup>-3</sup> as the constituents transported within the watermass, or delivered via sinking from above, undergo further remineralisation (Supplementary Figure 1). Using an age tracer within a data-constrained ocean circulation inverse model (OCIM)<sup>35</sup> that reproduces P16 salinity measurements, intermediate water in this density window aged by ~190 years (from 69 to 260 years) during this part of the P16 transect (Figure 1, see also Supplementary Figure 2).

As expected from our understanding of P biogeochemistry, PO<sub>4</sub> is well correlated with AOU within the intermediate water layer (R=0.96, Figure 2a) and the slope of 11.48±0.71 mmol P mol C<sup>-1</sup> is very close to that expected from the organic matter content<sup>36</sup>. The intercept indicates a preformed PO<sub>4</sub> concentration of 1.04±0.04 mmol m<sup>-3</sup> at the intermediate water outcrop in the Fe-limited Southern Ocean. More surprising is the broadly linear relationship between DFe and AOU within intermediate water (R=0.66, Figure 2b), with a slope of 3.92±0.99 µmol Fe mol C<sup>-1</sup> and a preformed DFe concentration of 0.16±0.06 µmol m<sup>-3</sup>. The Fe/C ratios estimated from the slope of the linear regression between Fe and AOU within AAIW are similar to those previously estimated from vertical profiles across the North Pacific Ocean 37,38. However, the profile-based estimates cannot strictly be used to quantify the accumulation of dFe since the zero AOU intercept that should represent the surface water outcrop of the isopycnal layer is instead the directly overlying surface water. This means that the values reported here are the first estimates of the temporal accumulation of DFe alongside concomitant oxygen consumption in Pacific intermediate waters. Indeed, we can use the watermass age estimate from OCIM to derive rates of accumulation of 6.75 µmol PO<sub>4</sub> m<sup>-3</sup> yr<sup>-1</sup> and 2.34 nmol dFe m<sup>-3</sup> yr<sup>-1</sup> between 46S and 10S.

While the accumulation of PO<sub>4</sub>, relative to C, conforms our prior understanding based on observations of P/C ratios from organic matter<sup>36</sup>, DFe accumulation appears very low, even for the Fe-poor South Pacific. Estimates of median phytoplankton Fe content from available synchrotron measurements (Table 1) range from 11.7 to 31.3 µmol Fe mol C<sup>-1</sup>, with a median value of ~15.7 µmol Fe mol C<sup>-1</sup> typical of the South Pacific. This indicates that only around a quarter (25%) of phytoplankton Fe is accumulating as DFe in intermediate waters due to regeneration. It is possible that living phytoplankton are not representative of the sinking detrital pool<sup>39</sup>, which could be addressed by examining Fe/C ratios within bulk particulate matter. However, particulate Fe also includes relatively inert lithogenic Fe, which would overestimate the labile (i.e. biotic) Fe content. To account for this, we estimated lithogenic Fe (see methods) from the only GEOTRACES particulate Fe dataset from the Pacific Ocean (stations west of the east Pacific rise on the zonal GP16 transect between Ecuador and Tahiti) using three different lithogenic models accounting for a range of end members from the Pacific basin<sup>23,24,40</sup>. After this correction, median

157 non-lithogenic Fe/C ratios within all particulate samples, shallower than the lightest intermediate water isopycnal, range from 48.2-196.4 µmol Fe mol C<sup>-1</sup>, while the median 158 P/C ratio is 12.73 mmol P mol C<sup>-1</sup> (Table 1). This particulate analysis shows that the 159 accumulation of dFe along the intermediate water pathway is only 2-8% of the non-160 161 lithogenic particulate Fe or ~25% of phytoplankton Fe. In contrast, as expected from the 162 two-component preformed-regenerated model of P cycling, 90% of the median particle P/C 163 ratio accumulates as PO<sub>4</sub> along the intermediate water pathway. This suggests that the 164 simple two component balance between regenerated and preformed pools that explains 165 the internal cycling of PO<sub>4</sub> is not applicable for Fe and the balance of subsurface 166 solubilisation and scavenging processes that control the net observable Fe 167 remineralisation remain unconstrained.

168

#### Controls on dissolved iron accumulation in intermediate waters

169 170 171

172

173

174

175

176

177

There are three main hypotheses to explain the mismatch between accumulation of DFe and the magnitude of phytoplankton and particulate Fe stocks that fuel DFe replenishment. The first hypothesis states that particulate Fe is not exported from the surface ocean and instead retained in the zone shallower than the upper bound of intermediate waters. The second hypothesis states that particulate Fe is exported out of the upper ocean but is not regenerated. Finally, the third hypothesis states that ample Fe is exported and regenerated, but strong scavenging of regenerated Fe leads to minor accumulation of DFe.

178 179 180

181

182

183

184 185

186 187

188

189 190

191 192

193

194

195

The first hypothesis can be rejected since although recycling of Fe in the upper ocean is significant, ample particulate Fe is exported from the surface ocean. Significant recycling of Fe in the upper mixed layer has been demonstrated from a variety of field studies and budget calculations<sup>5,10,19,41-43</sup>, which indicate substantial turnover of the particulate Fe pool. Measurements of particulate Fe exported from the upper ocean from trace metal clean sediment traps are very rare, but, where available, also support substantial export of particulate Fe. Sinking particulate Fe flux data from the SAZ-Sense and FeCycle I and II (at ~100m depth and either directly accounting for lithogenic Fe or taking a conservative 80% estimate of the lithogenic fraction<sup>44</sup>) results in non-lithogenic Fe/C export ratios of between 30-400 µmol Fe mol C<sup>-1</sup> and P/C export ratios of around 6-8.5 mmol P mol C<sup>-1</sup> across all data<sup>44-46</sup> (all broadly similar to those from non-lithogenic mixed layer particles, Table 1). Median values from both datasets produce flux ratios of 141.6 µmol Fe mol C<sup>-1</sup> and 5.6 mmol P mol C<sup>-1</sup>, compared to accumulation ratios of 3.9 µmol Fe mol C<sup>-1</sup> and 11.5 mmol P mol C<sup>-1</sup> (Table 1). Thus, despite intense recycling in the surface mixed layer, export fluxes of non-lithogenic Fe out of the base of the surface mixed layer are significant relative to the accumulation of DFe during regeneration along mode water pathways in the oceans' interior (Table 1), leading us to reject hypothesis one.

196 197 198

199

200

201

202

203

204

205

206

207

The second hypothesis can be rejected in light of previous assessments of solubilisation of Fe from particles below the mixed layer (at between 100-200m) through a set of experiments that incubated a subsurface particle assemblage resuspended from McLane pump 142mm filters and monitored the release of DFe, as well as by iron budget calculations. These estimates are sparse, but for two distinct field experiments, dFe release rates range between 511-1,314, and 120-460 nmol m<sup>-3</sup> yr<sup>-1</sup> from particles from below the mixed layer<sup>47,48</sup>. Budget based calculations are similar, producing subsurface dFe regeneration rates of 190-2,630 nmol m<sup>-3</sup> yr<sup>-1</sup> at 100m<sup>45</sup>. Across all estimates we find a median of 485 nmol m<sup>-3</sup> yr<sup>-1</sup>, two orders of magnitude greater than the dFe accumulation rate of ~2 nmol m<sup>-3</sup> yr<sup>-1</sup> we find within intermediate water (Table 1). These rates are clearly substantial, and we are required to reject hypothesis two.

208

210 Based on our rejection of the first two hypotheses, we are required to invoke a significant 211 loss of regenerated Fe from either scavenging or bacterial removal when considering hypothesis three. This would reconcile the low rates of dFe accumulation within 212 213 intermediate waters with the significant export of non-lithogenic Fe and large rates of dFe 214 solubilisation from sinking particles. The potential role of the removal of regenerated algal 215 biogenic Fe has been previously observed using synchrotron-mapping of particles derived from sediment traps<sup>49</sup> and would also explain new observations of an increasing 216 association of sinking non-lithogenic particulate Fe with authigenic phases in deep-moored 217 sediment traps (between 500, 1,500 and 3,200m) in the Atlantic<sup>50</sup>. For the Pacific, we 218 calculate that 20-40% of the particulate Fe within the intermediate water in the western 219 220 portion of the GP16 Pacific section cannot be accounted for by the sum of lithogenic and 221 algal biogenic components. This implies a non-negligible authigenic particulate Fe 222 component that would be consistent with removal of regenerated Fe by scavenging.

# **Discussion**

209

223224

225226

227

228

229

230

231

232

233

234

235

236237

238

239

240

241242

243

244

245

246

247248249

250

251

252

253

254255

256257

258

259

260

Our results point to continual removal of regenerated iron, resulting in only a small accumulation of DFe within intermediate waters. The combination of the constant rain of new material and the disaggregation of sinking particles in the ocean interior may be able to maintain scavenging of released Fe as the increasing surface area:volume ratio provides new surfaces for scavenging. Indeed, the increase in the flux of small particles (11-64 μm, equivalent spherical diameter, ESD) off Bermuda, and the concomitant opposite trend for large (> 64 μm ESD) particles at depth<sup>51</sup>, highlights the important role this may play in producing small particles. Similarly, number spectrum analyses (using underwater video cameras) across the upper 200 m of the water column in the S. Pacific Gyre reveal much higher abundances of small particles than larger ones<sup>52</sup>. As scavenging of trace metals like Fe is highly dependent on surface area 53-55, these particle disaggregation/fragmentation processes can catalyse further scavenging of the dFe released by regeneration. Scavenging of regenerated Fe into authigenic phases may also enhance particle sinking rates by increasing the specific gravity of particles (as noted for lithogenic Fe<sup>56</sup>). These abiotic processes may act in concert with the removal of solubilised Fe by heterotrophic bacteria operating within particle microenvironments<sup>57,58</sup>. If we take our median estimated regeneration rate of dFe and the estimated accumulation rate of dFe (Table 1), and then combining these with a typical intermediate water layer thickness of 300m at 10S, requires net downward removal fluxes of around 0.39 μmol m<sup>-2</sup> d<sup>-1</sup>. Although these fluxes would be inconspicuous in the measurements spanning around 0.4-10 µmol m<sup>-2</sup> d<sup>-1</sup> from trace metal clean sediment traps<sup>44,45</sup>, they are crucial in shaping the basin scale internal cycling of dFe in intermediate water layers.

We observe a small, but significant, accumulation of DFe with time (Figure 2b), suggesting that the net regeneration quantified by the slope of the DFe versus AOU relationship integrates the regeneration and scavenging fluxes. Observed concentrations of weak Febinding ligands are typically well in excess of DFe levels, which would imply an ample capacity to stabilise regenerated Fe at much higher levels<sup>59-62</sup> and is not in agreement with our analysis. However, the muted increase in DFe we observe is very consistent with the apparent saturation of strong Fe-binding ligands by DFe pools in the south Pacific Ocean<sup>60</sup>. This would imply that strong Fe-binding ligands, rather than their weaker counterparts, may play a key role in shaping the dissolved Fe distribution in the oceans' interior. An additional role may be played by the interplay between soluble and colloidal iron pools, which can also be part of the ligand pools<sup>20-22</sup>. For instance, in the future it may be useful to compare the net regeneration from the DFe-AOU slope to observations of

colloidal iron. Finally, we emphasise that the putative production of authigenic Fe from the DFe solubilised during regeneration, that we term here as scavenging, might not occur in the water column, but instead within particles and their associated microenvironments<sup>57,58</sup> in a manner disconnected from the wider water column ligand pool.

264265266

267268

269

270

271

272273

274

275

276

277

278

279

280

281

261

262

263

The DFe-AOU slope of 2.7 µmol DFe mol AOU<sup>-1</sup> from our analysis (Figure 2b) permits us to examine what proportion of the DFe pool might be controlled by the net interplay between regeneration and scavenging (termed 'internal cycling' hereon). Roughly twothirds of the interior PO<sub>4</sub> signal is preformed (controlled by physical transport), with the remaining one-third due to regeneration<sup>27,28</sup>. In contrast to PO<sub>4</sub>, the proportion of the DFe pool controlled by internal cycling in intermediate waters (within the 26.8-27.2 isopycnal layer) across the entire available GEOTRACES dataset<sup>26</sup> of DFe and AOU has a median value of 0.57 (Figure 3). This implies that over half of the DFe concentration in intermediate water is in fact set by internal cycling (i.e. the interplay between regeneration and scavenging), with the remainder controlled by physical transport of preformed DFe (either from the ocean surface or laterally). The stronger role played by preformed PO<sub>4</sub> than preformed DFe arises due to the higher unused PO<sub>4</sub> levels in the, typically Fe-limited, watermass outcrop regions. Thus, because DFe is drawn down to very low levels in regions of intermediate water formation, internal cycling has a larger imprint on the interior DFe concentrations across much of the globe than for PO<sub>4</sub>. This view agrees with the lack of clear water mass signals in large scale ocean DFe sections<sup>63</sup> and is at odds with simulations from early iron models that retained a large physically transported component.

282 283 284

285

286

287

288

289

290

291

292

293

294

295

296

297

298

299

300

301 302

303

304

305

Overall, the strong mismatch we find between the internal basin scale Fe cycle fluxes and the residual DFe pool that accumulates from their interplay explains why Fe models can produce such divergent residence times while trying to reproduce the same dFe datasets. Our analysis finds DFe to be rapidly cycled by regeneration and scavenging, which supports those models parameterised with short residence times. The net regeneration that shapes the multi-decade accumulation of DFe in intermediate waters is likely controlled by some combination of strong iron binding ligands, colloidal dynamics and authigenic iron pools. Because of the dominance of internal cycling, the concentration of Fe, relative to major nutrients N and P, and hence upper ocean iron limitation, will be strongly sensitive to small changes in the gross fluxes of regeneration and scavenging. For instance, the iron content of upper ocean phytoplankton is highly variable and fluctuations due to changing iron supply or phytoplankton species composition will affect the gross regeneration fluxes. Alternatively, biological and chemical transformations of particles, strong iron-binding ligands and/or iron speciation will modify gross scavenging rates. Both these examples would change the net regeneration rate and hence the relative to supply of DFe to the upper ocean biota. Our isopycnal framework provides a mechanistic methodology to assess ocean biogeochemical models more rigorously in future model evaluation efforts. A new generation of in situ processes studies<sup>1</sup>, tracking the evolution of Fe biogeochemistry, measuring both fluxes and particulate and dissolved Fe pools within a coherent physical framework would offer the potential to further constrain the internal cycling mechanisms for inclusion into global biogeochemical models. This improved mechanistic understanding of the ocean Fe cycle is required to reduce uncertainties in how changes in climate will affect surface ocean Fe limitation of primary productivity.

306 307

#### **Methods**

308 309 310

311

312

#### Field sampling and data processing

Sampling along the CLIVAR P16 section was conducted during two cruises, from Tahiti to Kodiak, Alaska aboard the R/V Thomas Thompson (9<sup>th</sup> January – 22 February 2005;

P16N), and from Tahiti to Antarctica aboard the R/V Roger Revelle (15<sup>th</sup> February – 25<sup>th</sup> 313 314 March 2006; P16S). Samples for dFe were analysed following previously published protocols<sup>64</sup>. Briefly, 15 mL aliquots of acidified (0.024 M, HCl) sample were spiked with 315 100 µL of an <sup>57</sup>Fe isotope enriched solution (Fe concentration of 177 nM) and UV-oxidised 316 317 (>1 h). After cooling overnight, samples were buffered with ammonium acetate to pH 6.4 ± 318 0.2 prior to being passed through a column packed with Toyopearl AF-Chelate-650M. 319 Extracted Fe was subsequently eluted with 1 M HNO<sub>3</sub> into 1 mL aliquots and analysed by 320 High Resolution-Inductively Coupled Plasma-Mass Spectrometry (Thermo Finnigan 321 Element 1). dFe concentrations were quantified using a standard isotope dilution 322 equation. The analytical limit of detection (LOD; 3xSD of blank) averaged 0.019 nM (n=20) 323 during the analysis period, while the procedural LOD (based on 3xSD of replicate analysis 324 of SAFe S1) averaged 0.034 nM (n=29). Accuracy and precision was assessed through the replicate extraction and analysis of SAFE and GEOTRACES seawater reference 325 326 materials<sup>64</sup>. Typical within run precision averaged 2.2% (1RSD, n=27) at iron 327 concentrations around 1 nM and 11.8% (1RSD, n=29) at lower iron concentrations (~0.1 328 nM). AOU was calculated from oxygen saturation (derived using temperature and salinity). 329 DFe, PO<sub>4</sub> and AOU were binned within the intermediate water density layers (28.6-27.2) 330 and between latitudes of 46S and 10S. Statistics were performed using Type II 331 regressions via the R package 'lmodel2'. The net regeneration (Fe<sub>REG</sub>') that results from 332 the near-balance between regeneration and scavenging is derived by combining the Fe / 333 AOU slope from the P16 with AOU using oxygen, temperature, salinity and DFe data from IDP2017<sup>26</sup> between the 26.8-27.2 isopycnal layer that represents intermediate water. Field 334 335 data from the P16 voyage is available from BCO-DMO. 336

# Corrections for Lithogenic and algal Biogenic Fe

337

338

339

340

341

342

343

344

345

346

347

348349

350

351

352

353

354

355

356 357

Presuming that total particulate Fe in any sample is the sum of algal biogenic (PFeBio, Passociated), lithogenic (PFeLith, AI- or Ti-associated), and scavenged sub-fractions, we estimate scavenged Fe (PFeScav) by sequentially subtracting estimated lithogenic (PFeLitho), non-lithogenic (PFeNonLitho) and authigenic (PFeAuth) fractions via the following three balances: PFeTotal = PFeLitho + PFeBio + PFeScav, PFeNonLitho = PFeTotal – PFeLitho and PFeAuth = PFeNonLitho – PFeBio. In this study we based lithogenic Fe corrections on two assumptions: 1) lithogenic material in the ocean is ultimately derived from a crustal source(s) with estimable, fixed composition(s), and 2) lithogenic particles are refractory, meaning that elemental exchange with dissolved or other particulate pools during their marine residence times (weeks to years)<sup>24</sup> does not significantly alter their composition. To estimate and correct for lithogenic Fe we quantify the number and composition of potential lithogenic end-members. Via the ratios of Al, Ti and Th we address the compositional gradients of lithogenic particles in the GP16 transect and estimate the fractional composition of each end-member (see Supplementary Note and Supplementary Figures 3 and 4). We then correct for lithogenic Fe using Fe/Al or Fe/Ti ratio(s) from one or more end-member(s) in turn for a total of three lithogenic Fe estimates. Finally, algal biogenic Fe (PFeBio), is derived from particulate phosphorus (PP) concentrations and estimates of the algal biogenic Fe/P ratio. This analysis is performed using data from the GP16 section from the GEOTRACES IDP2017<sup>26</sup>.

# Acknowledgements

 This study was initiated during the visit of A.T. to the University of Tasmania (Australia), supported by a University of Tasmania Visiting Scholar award and by a European Research Council grant to A.T. (project ID 724289). A.R.B was supported by the Australian Research Council (FT130100037 and DP150100345) and the Antarctic Climate and Ecosystems Cooperative Research Centre. M.J.E (DP170102108) and P.W.B (FL160100131 and DP170102108) were supported by the Australian Research Council. Collection of CLIVAR iron data used in this work was supported by three NSF OCE grants (0223378, 0649639 and 0752832). A portion of this work was performed at the National High Magnetic Field Laboratory, which is supported by National Science Foundation Cooperative Agreement No. DMR-1157490 and the State of Florida. B.S.T and D.C.O were supported by NSF OCE grants 1232814 and 1435862. We thank Bob Anderson for helpful comments, Chris Measures, Matt Brown, Bill Hiscock, Amy Apprill, Lyle Leonard, Clifton Buck and Paul Hansard for helping collect the dissolved iron samples on P16. Field data from the P16 voyage is available from BCO-DMO. We thank Bob Anderson for constructive comments on an earlier version of this manuscript.

#### **Author Contributions**

The study was designed by A.T and P.W.B, with input from M.J.E and A.R.B. A.T conducted the analysis. W.M.L and A.M provided datasets from P16. B.S.T and D.C.O analysed phytoplankton and particulate datasets. T.D performed the ocean circulation model inversion. The paper was written by A.T and P.W.B, with contributions from all coauthors.

# **Competing interests**

386 The authors declare no competing interests.

# Figure Captions:

**Figure 1**. Study Area. The southern part of the CLIVAR P16S line in the south Pacific Ocean, on a backdrop of water age (years) from the OCIM model for the intermediate water isopycnal layer ( $\sigma_0$ =26.8-27.2). The individual stations used in this analysis are marked with red crosses.

**Figure 2**. Linking phosphate and dissolved iron to apparent oxygen utilisation. Plots of PO<sub>4</sub> (phosphate) and DFe (dissolved iron) observations against AOU (apparent oxygen utilisation) observations between the  $\sigma_0$ = 26.8-27.0 isopycnal layers along the P16 transect through the South Pacific Ocean, performed with a Type II regression

**Figure 3.** Origins of dissolved iron in IDP2017. The fraction of the dissolved iron concentration from the IDP2017 explained by the regeneration – scavenging balance between the  $\sigma_0$ = 26.8-27.0 isopycnal layers is quantified here. The magnitude of the regeneration – scavenging balance (in Fe<sub>R</sub>, mol m<sup>-3</sup>) can be derived by using the slope of the apparent oxygen utilisation – dissolved iron relationship from the P16 transect (2.7 µmol dissolved iron mol apparent oxygen utilisation <sup>-1</sup>) and the independent apparent oxygen utilisation and dissolved iron datasets from the GEOTRACES IDP2017. The net regeneration of dissolved iron (Fe<sub>R</sub>) is then divided by the observed total dissolved iron to quantify the fraction explained by the regeneration – scavenging balance. The median value of 0.57 is indicated with a vertical dashed line. This indicates that over half of the observed dissolved iron is explained by the regeneration – scavenging balance.

 **Table 1.** Meta-analysis of median and inter-quartile ranges (IQR) stoichiometric ratios from phytoplankton, particles (with different lithogenic corrections applied), sediment trap fluxes (with local estimates of lithogenic Fe or applying a conservative 80% lithogenic correction) and below mixed layer regeneration rates from process studies. Median ratios and slopes are in units of  $\mu$ mol/mol (Fe/C) or mmol/mol (P/C), while rates are either nmol dFe m<sup>-3</sup> yr<sup>-1</sup> or  $\mu$ mol PO<sub>4</sub> m<sup>-3</sup> yr<sup>-1</sup>

		Fe/C		P/C	
	Detail	Median	IQR	Median	IQR
Phyto-	South tropical Pacific	16.0	7.8-40.7		
plankton	South Pacific <sup>65</sup>	15.3	9.7-26.5		
	Equatorial Pacific <sup>66</sup>	11.7	6.9-20.4		
	North Pacific	20.2	9.8-55.0		
	North Atlantic <sup>67</sup>	31.3	19.8-59.9		
Marine	Ti endmember	48.21	2.67-204.76	12.73	11.38-14.55
Particles*	Al endmember	196.4	105.5-396.7		
	Al/Ti endmember	103.35	56.69-175.83		
		Fe/C		P/C	
		Median	IQR	Median	IQR
Export <sup>^</sup>	SAZ-Sense, FeCycle	141.6	190.6	5.6	3.6
	I and II sediment traps <sup>44-46</sup>				
		Fe rate			
		Median	IQR		
Regener- ation <sup>~</sup>	Experiments and budgets <sup>45,47,48</sup>	485.5	855.9		
	<u> </u>	Fe/C	Fe Rate	P/C	P Rate
Dissolved	Intermediate water	3.92	2.34	11.48	6.75
		±0.99		±0.71	

\*particles collected from bottles during GEOTRACES GP16 voyage between Ecuador and Tahiti in the south Pacific above the intermediate water layer and west of station 23 to avoid influence of low oxygen waters (n=54).

^Calculated non-lithogenic flux from sediment traps from the SAZ-Sense, FeCycle I and FeCycle II process studies, either by using local corrections or a conservative estimate of 80% lithogenic Fe (n=14 for Fe and 11 for P).

Regeneration rates are compiled from all direct measurements of solubilization of particles collected from below the mixed layer and iron budget calculations of iron regeneration (n=6).

#### **Data Availability**

All the data used in this research are freely available and may be downloaded through the links detailed in the Methods section.

437	Refer	ences
438 439 440	1	Tagliabue, A. <i>et al.</i> The integral role of iron in ocean biogeochemistry. <i>Nature</i> <b>543</b> , 51-59, doi:10.1038/nature21058 (2017).
441 442	2	Moore, C. M. <i>et al.</i> Large-scale distribution of Atlantic nitrogen fixation controlled by iron availability. <i>Nature Geoscience</i> <b>2</b> , 867-871, doi:10.1038/ngeo667 (2009).
443 444 445	3	Browning, T. J. <i>et al.</i> Iron limitation of microbial phosphorus acquisition in the tropical North Atlantic. <i>Nature communications</i> <b>8</b> , 15465, doi:10.1038/ncomms15465 (2017).
446 447 448	4	Moore, C. M. Diagnosing oceanic nutrient deficiency. <i>Philosophical transactions</i> . <i>Series A, Mathematical, physical, and engineering sciences</i> <b>374</b> , doi:10.1098/rsta.2015.0290 (2016).
449 450	5	Tagliabue, A. <i>et al.</i> Surface-water iron supplies in the Southern Ocean sustained by deep winter mixing. <i>Nature Geoscience</i> <b>7</b> , 314-320, doi:10.1038/ngeo2101 (2014).
451 452 453	6	Sarmiento, J. L., Gruber, N., Brzezinski, M. A. & Dunne, J. P. High-latitude controls of thermocline nutrients and low latitude biological productivity. <i>Nature</i> <b>427</b> , 56-60, doi:10.1038/nature02127 (2004).
454 455 456	7	Tagliabue, A. <i>et al.</i> How well do global ocean biogeochemistry models simulate dissolved iron distributions? <i>Global Biogeochemical Cycles</i> , doi:10.1002/2015gb005289 (2016).
457 458 459	8	Parekh, P., Follows, M. J. & Boyle, E. A. Decoupling of iron and phosphate in the global ocean. <i>Global Biogeochemical Cycles</i> <b>19</b> , doi:10.1029/2004gb002280 (2005).
460 461	9	Archer, D. E. & Johnson, K. A model of the iron cycle in the ocean. <i>Global Biogeochemical Cycles</i> <b>14</b> , 269-279, doi:10.1029/1999gb900053 (2000).
462 463 464	10	Boyd, P. W., Ellwood, M. J., Tagliabue, A. & Twining, B. S. Biotic and abiotic retention, recycling and remineralization of metals in the ocean. <i>Nature Geoscience</i> <b>10</b> , 167-173, doi:10.1038/ngeo2876 (2017).
465 466 467	11	Leung, S., Cabré, A. & Marinov, I. A latitudinally banded phytoplankton response to 21st century climate change in the Southern Ocean across the CMIP5 model suite. <i>Biogeosciences</i> <b>12</b> , 5715-5734, doi:10.5194/bg-12-5715-2015 (2015).
468 469 470	12	Cabré, A., Marinov, I. & Leung, S. Consistent global responses of marine ecosystems to future climate change across the IPCC AR5 earth system models. <i>Climate Dynamics</i> , doi:10.1007/s00382-014-2374-3 (2014).
471 472 473	13	Misumi, K. <i>et al.</i> The iron budget in ocean surface waters in the 20th and 21st centuries: projections by the Community Earth System Model version 1. <i>Biogeosciences</i> <b>11</b> , 33-55, doi:10.5194/bg-11-33-2014 (2014).
474 475 476	14	Bopp, L. <i>et al.</i> Multiple stressors of ocean ecosystems in the 21st century: projections with CMIP5 models. <i>Biogeosciences</i> <b>10</b> , 6225-6245, doi:10.5194/bg-10-6225-2013 (2013).

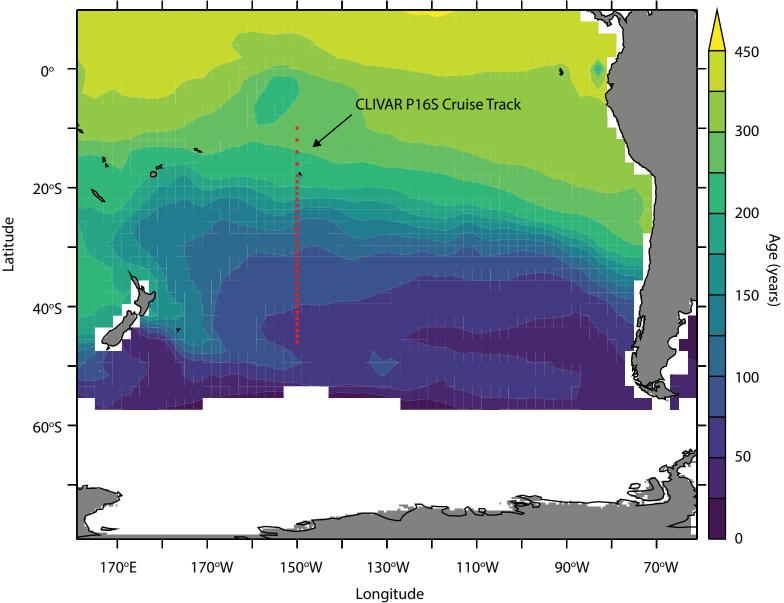
477 478 479	15	Laufkötter, C. <i>et al.</i> Drivers and uncertainties of future global marine primary production in marine ecosystem models. <i>Biogeosciences</i> <b>12</b> , 6955-6984, doi:10.5194/bg-12-6955-2015 (2015).
480 481	16	Boyd, P. W. & Ellwood, M. J. The biogeochemical cycle of iron in the ocean. <i>Nature Geoscience</i> <b>3</b> , 675-682, doi:10.1038/ngeo964 (2010).
482 483 484 485	17	German, C. R. <i>et al.</i> Hydrothermal impacts on trace element and isotope ocean biogeochemistry. <i>Philosophical Transactions of the Royal Society A: Mathematical, Physical and Engineering Sciences</i> <b>374</b> , 20160035, doi:10.1098/rsta.2016.0035 (2016).
486 487 488 489	18	Homoky, W. B. <i>et al.</i> Quantifying trace element and isotope fluxes at the ocean–sediment boundary: a review. <i>Philosophical Transactions of the Royal Society A: Mathematical, Physical and Engineering Sciences</i> <b>374</b> , 20160246, doi:10.1098/rsta.2016.0246 (2016).
490 491 492	19	Boyd, P. W. <i>et al.</i> Why are biotic iron pools uniform across high- and low-iron pelagic ecosystems? <i>Global Biogeochemical Cycles</i> <b>29</b> , 1028-1043, doi:10.1002/2014gb005014 (2015).
493 494 495	20	Wu, J., Boyle, E., Sunda, W. & Wen, L. S. Soluble and colloidal iron in the oligotrophic North Atlantic and North Pacific. <i>Science</i> <b>293</b> , 847-849, doi:10.1126/science.1059251 (2001).
496 497 498 499	21	Nishioka, J., Takeda, S., Wong, C. S. & Johnson, W. K. Size-fractionated iron concentrations in the northeast Pacific Ocean: distribution of soluble and small colloidal iron. <i>Marine Chemistry</i> <b>74</b> , 157-179, doi:10.1016/s0304-4203(01)00013-5 (2001).
500 501 502	22	Fitzsimmons, J. N. & Boyle, E. A. Both soluble and colloidal iron phases control dissolved iron variability in the tropical North Atlantic Ocean. <i>Geochimica et Cosmochimica Acta</i> <b>125</b> , 539-550, doi:10.1016/j.gca.2013.10.032 (2014).
503 504 505	23	Lam, P. J. <i>et al.</i> Size-fractionated distributions of suspended particle concentration and major phase composition from the U.S. GEOTRACES Eastern Pacific Zonal Transect (GP16). <i>Marine Chemistry</i> , doi:10.1016/j.marchem.2017.08.013 (2017).
506 507 508	24	Ohnemus, D. C. & Lam, P. J. Cycling of lithogenic marine particles in the US GEOTRACES North Atlantic transect. <i>Deep Sea Research Part II: Topical Studies in Oceanography</i> <b>116</b> , 283-302, doi:10.1016/j.dsr2.2014.11.019 (2015).
509 510	25	Mawji, E. et al. The GEOTRACES Intermediate Data Product 2014. <i>Marine Chemistry</i> <b>177</b> , 1-8, doi:10.1016/j.marchem.2015.04.005 (2015).
511 512	26	Schlitzer, R. et al. The GEOTRACES Intermediate Data Product 2017. Chemical Geology 493, 210-223, doi:10.1016/j.chemgeo.2018.05.040 (2018).
513 514 515 516	27	Broecker, W. S., Takahashi, T. & Takahashi, T. Sources and flow patterns of deep-ocean waters as deduced from potential temperature, salinity, and initial phosphate concentration. <i>Journal of Geophysical Research</i> <b>90</b> , 6925, doi:10.1029/JC090iC04p06925 (1985).

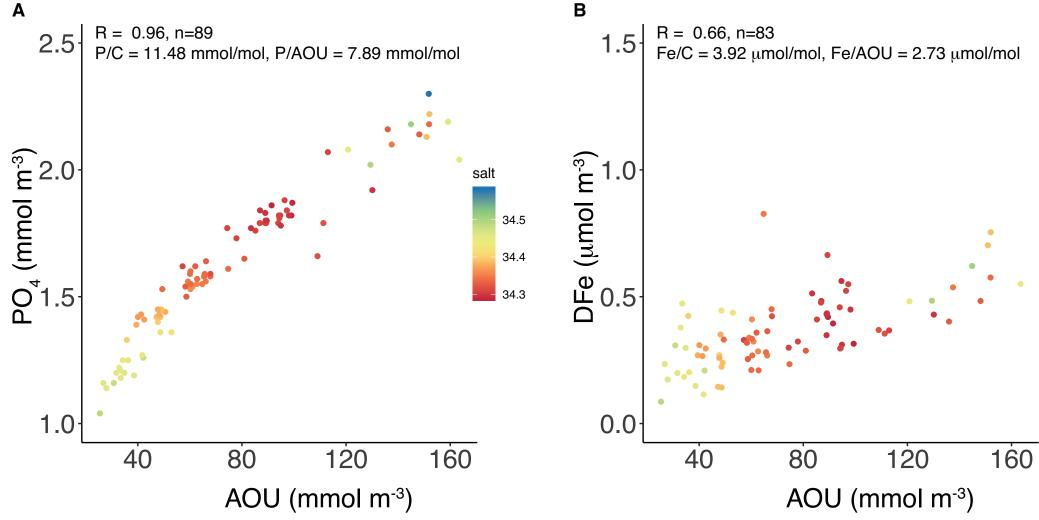
517 518 519	28	Ito, T. & Follows, M. J. Preformed phosphate, soft tissue pump and atmospheric CO2. <i>Journal of Marine Research</i> <b>63</b> , 813-839, doi:10.1357/0022240054663231 (2005).		
520 521 522	29	Johnson, K. S., Gordon, R. M. & Coale, K. H. What controls dissolved iron concentrations in the world ocean? <i>Marine Chemistry</i> <b>57</b> , 137-161, doi:10.1016/s0304-4203(97)00043-1 (1997).		
523 524 525	30	Hayes, C. T. <i>et al.</i> Replacement Times of a Spectrum of Elements in the North Atlantic Based on Thorium Supply. <i>Global Biogeochemical Cycles</i> <b>32</b> , 1294-1311, doi:10.1029/2017gb005839 (2018).		
526 527 528	31	Hayes, C. T. <i>et al.</i> Thorium isotopes tracing the iron cycle at the Hawaii Ocean Time-series Station ALOHA. <i>Geochimica et Cosmochimica Acta</i> <b>169</b> , 1-16, doi:10.1016/j.gca.2015.07.019 (2015).		
529 530 531 532	32	Hartin, C. A. <i>et al.</i> Formation rates of Subantarctic mode water and Antarctic intermediate water within the South Pacific. <i>Deep Sea Research Part I: Oceanographic Research Papers</i> <b>58</b> , 524-534, doi:10.1016/j.dsr.2011.02.010 (2011).		
533 534 535	33	Sloyan, B. M. & Rintoul, S. R. Circulation, renewal, and modification of Antarctic mode and intermediate water. <i>Journal of Physical Oceanography</i> <b>31</b> , 1005-1030, doi:Doi 10.1175/1520-0485(2001)031<1005:Cramoa>2.0.Co;2 (2001).		
536 537	34	Talley, L. D. in <i>The South Atlantic: Present and Past Circulation</i> 219-238 (Springer Berlin Heidelberg, 1996).		
538 539 540	35	DeVries, T. The oceanic anthropogenic CO2sink: Storage, air-sea fluxes, and transports over the industrial era. <i>Global Biogeochemical Cycles</i> <b>28</b> , 631-647, doi:10.1002/2013gb004739 (2014).		
541 542	36	Moreno, A. R. & Martiny, A. C. Ecological Stoichiometry of Ocean Plankton. <i>Annual review of marine science</i> , doi:10.1146/annurev-marine-121916-063126 (2017).		
543 544 545	37	Sunda, W. G. Control of dissolved iron concentrations in the world ocean, A comment. <i>Marine Chemistry</i> <b>57</b> , 169-172, doi:10.1016/s0304-4203(97)00045-5 (1997).		
546 547 548	38	Martin, J. H., Gordon, R. M., Fitzwater, S. & Broenkow, W. W. Vertex - Phytoplankton Iron Studies in the Gulf of Alaska. <i>Deep-Sea Res</i> <b>36</b> , 649-&, doi:10.1016/0198-0149(89)90144-1 (1989).		
549 550 551 552 553	39	Wilson, S. E., Steinberg, D. K. & Buesseler, K. O. Changes in fecal pellet characteristics with depth as indicators of zooplankton repackaging of particles in the mesopelagic zone of the subtropical and subarctic North Pacific Ocean. <i>Deep Sea Research Part II: Topical Studies in Oceanography</i> <b>55</b> , 1636-1647, doi: <a href="https://doi.org/10.1016/j.dsr2.2008.04.019">https://doi.org/10.1016/j.dsr2.2008.04.019</a> (2008).		
554 555 556	40	van der Merwe, P. <i>et al.</i> Sourcing the iron in the naturally fertilised bloom around the Kerguelen Plateau: particulate trace metal dynamics. <i>Biogeosciences</i> <b>12</b> , 739-755, doi:10.5194/bg-12-739-2015 (2015).		

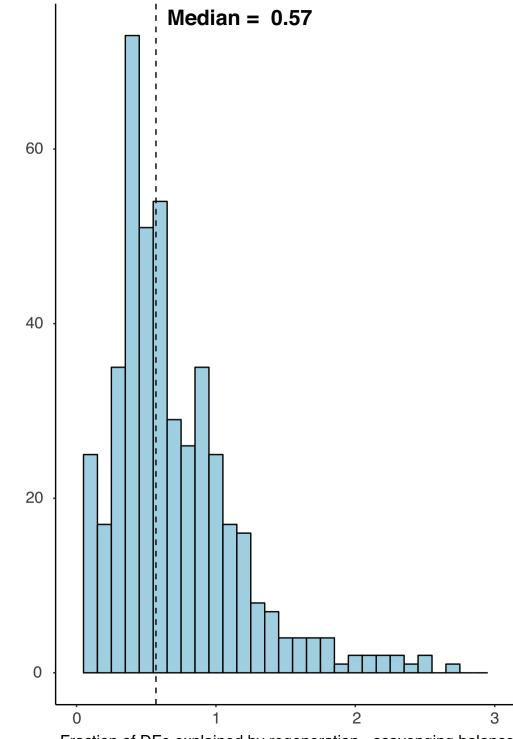
557 41 Strzepek, R. F. et al. Spinning the "Ferrous Wheel": The importance of the microbial community in an iron budget during the FeCycle experiment. Global 558 559 Biogeochemical Cycles 19, GB4S26, doi:10.1029/2005gb002490 (2005). 560 42 Boyd, P. W. et al. Microbial control of diatom bloom dynamics in the open ocean. 561 Geophysical Research Letters 39, doi:10.1029/2012gl053448 (2012). 562 43 Tovar-Sanchez, A., Duarte, C. M., Hernández-León, S. & Sañudo-Wilhelmy, S. A. 563 Krill as a central node for iron cycling in the Southern Ocean. Geophysical 564 Research Letters 32, doi:10.1029/2006gl029096 (2007). 44 Frew, R. D. et al. Particulate iron dynamics during FeCycle in subantarctic waters 565 southeast of New Zealand. Global Biogeochemical Cycles 20, 566 567 doi:10.1029/2005gb002558 (2006). 45 Ellwood, M. J. et al. Pelagic iron cycling during the subtropical spring bloom, east of 568 New Zealand. Marine Chemistry 160, 18-33, doi:10.1016/j.marchem.2014.01.004 569 570 (2014).571 46 Bowie, A. R. et al. Biogeochemical iron budgets of the Southern Ocean south of 572 Australia: Decoupling of iron and nutrient cycles in the subantarctic zone by the summertime supply. Global Biogeochemical Cycles 23, doi:10.1029/2009gb003500 573 574 (2009).575 47 Boyd, P. W., Ibisanmi, E., Sander, S. G., Hunter, K. A. & Jackson, G. A. 576 Remineralization of upper ocean particles: Implications for iron biogeochemistry. Limnology and Oceanography 55, 1271-1288, doi:10.4319/lo.2010.55.3.1271 577 578 (2010).579 48 Velasquez, I. B. et al. Ferrioxamine Siderophores Detected amongst Iron Binding 580 Ligands Produced during the Remineralization of Marine Particles. Frontiers in 581 Marine Science 3, doi:10.3389/fmars.2016.00172 (2016). 582 49 Twining, B. S. et al. Differential remineralization of major and trace elements in 583 sinking diatoms. Limnol. Oceanogr 59, 689-704, doi:10.4319/lo.2014.59.3.0689 584 (2014).50 Conte, M. H., Carter, A. M., Koweek, D. A., Huang, S. & Weber, J. C. The elemental 585 586 composition of the deep particle flux in the Sargasso Sea. Chemical Geology, 587 doi:10.1016/j.chemgeo.2018.11.001 (2018). 51 588 Durkin, C. A., Estapa, M. L. & Buesseler, K. O. Observations of carbon export by 589 small sinking particles in the upper mesopelagic. Marine Chemistry 175, 72-81, 590 doi:https://doi.org/10.1016/j.marchem.2015.02.011 (2015). 52 591 Stemmann, L. et al. Volume distribution for particles between 3.5 to 2000 µm in the 592 upper 200 m region of the South Pacific Gyre. *Biogeosciences* **5**, 299-310, 593 doi:10.5194/bg-5-299-2008 (2008). 594 53 Honeyman, B. D., Balistrieri, L. S. & Murray, J. W. Oceanic trace metal scavenging: 595 the importance of particle concentration. Deep Sea Research Part A. Oceanographic Research Papers 35, 227-246, doi:10.1016/0198-0149(88)90038-6 596 597 (1988).

598 54 Honeyman, B. D. & Santschi, P. H. A Brownian-pumping model for oceanic trace 599 metal scavenging: Evidence from Th isotopes. Journal of Marine Research 47, 951-600 992, doi:10.1357/002224089785076091 (1989). 601 55 Jannasch, H. W., Honeyman, B. D. & Murray, J. W. Marine scavenging: The relative 602 importance of mass transfer and reaction rates. Limnology and Oceanography 41, 603 82-88, doi:10.4319/lo.1996.41.1.0082 (1996). 604 56 Ternon, E. et al. The impact of Saharan dust on the particulate export in the water column of the North Western Mediterranean Sea. *Biogeosciences* 7, 809-826, 605 606 doi:10.5194/bg-7-809-2010 (2010). 607 57 Alldredge, A. L. & Cohen, Y. Can Microscale Chemical Patches Persist in the Sea? Microelectrode Study of Marine Snow, Fecal Pellets. Science 235, 689-691, 608 609 doi:10.1126/science.235.4789.689 (1987). 58 610 Bianchi, D., Weber, T. S., Kiko, R. & Deutsch, C. Global niche of marine anaerobic 611 metabolisms expanded by particle microenvironments. Nature Geoscience 11, 263-268, doi:10.1038/s41561-018-0081-0 (2018). 612 613 59 Boyd, P. W. & Tagliabue, A. Using the L\* concept to explore controls on the 614 relationship between paired ligand and dissolved iron concentrations in the ocean. Marine Chemistry 173, 52-66, doi:10.1016/j.marchem.2014.12.003 (2015). 615 616 60 Buck, K. N., Sedwick, P. N., Sohst, B. & Carlson, C. A. Organic complexation of iron 617 in the eastern tropical South Pacific: Results from US GEOTRACES Eastern Pacific Zonal Transect (GEOTRACES cruise GP16). *Marine Chemistry*. 618 619 doi:10.1016/j.marchem.2017.11.007 (2017). 620 61 Buck, K. N., Sohst, B. & Sedwick, P. N. The organic complexation of dissolved iron 621 along the U.S. GEOTRACES (GA03) North Atlantic Section. Deep Sea Research 622 Part II: Topical Studies in Oceanography 116, 152-165, 623 doi:10.1016/j.dsr2.2014.11.016 (2015). 624 62 Gerringa, L. J. A., Rijkenberg, M. J. A., Schoemann, V., Laan, P. & de Baar, H. J. W. Organic complexation of iron in the West Atlantic Ocean. *Marine Chemistry* 177, 625 626 434-446, doi:10.1016/j.marchem.2015.04.007 (2015). 627 63 Rijkenberg, M. J. A. et al. Fluxes and distribution of dissolved iron in the eastern 628 (sub-) tropical North Atlantic Ocean. Global Biogeochemical Cycles 26. 629 doi:10.1029/2011gb004264 (2012). 630 64 Milne, A., Landing, W., Bizimis, M. & Morton, P. Determination of Mn, Fe, Co, Ni, Cu. Zn. Cd and Pb in seawater using high resolution magnetic sector inductively 631 coupled mass spectrometry (HR-ICP-MS). Analytica chimica acta 665, 200-207, 632 633 doi:10.1016/j.aca.2010.03.027 (2010). 634 65 King, A. L. et al. A comparison of biogenic iron quotas during a diatom spring bloom 635 using multiple approaches. Biogeosciences 9, 667-687, doi:10.5194/bg-9-667-2012 636 (2012).637 66 Twining, B. S. et al. Metal quotas of plankton in the equatorial Pacific Ocean. Deep-Sea Res Pt li 58, 325-341, doi:10.1016/j.dsr2.2010.08.018 (2011). 638

Twining, B. S., Rauschenberg, S., Morton, P. L. & Vogt, S. Metal contents of phytoplankton and labile particulate material in the North Atlantic Ocean. *Progress in Oceanography* **137**, 261-283, doi:10.1016/j.pocean.2015.07.001 (2015).







Frequency

Fraction of DFe explained by regeneration - scavenging balance